A computer-assisted verification of hyperchaos in the Saito hysteresis chaos generator

2006 J. Phys. A: Math. Gen. 39 9139

(http://iopscience.iop.org/0305-4470/39/29/009)

INSTITUTE OF PHYSICS PUBLISHING JOURNAL OF PHYSICS A: MATHEMATICAL AND GENERAL

J. Phys. A: Math. Gen. **39** (2006) 9139–9150 doi:10.1088/0305-4470/39/29/009

A computer-assisted verification of hyperchaos in the Saito hysteresis chaos generator

Qingdu Li[1] **and Xiao-Song Yang**[2,3]

[1] Institute for Nonlinear Systems, Chongqing University of Posts and Telecomm., Chongqing 400065, People's Republic of China
[2] Department of Mathematics, Huazhong University of Science and Technology, Wuhan 430074, People's Republic of China

E-mail: qingdu_li@163.com and yangxs@cqupt.edu.cn

Received 15 January 2006, in final form 4 June 2006
Published 5 July 2006
Online at stacks.iop.org/JPhysA/39/9139

Abstract
This paper presents a computer-assisted verification of hyperchaos in the well-known Saito hysteresis chaos generator (SHCG) by virtue of topological horseshoe theory. By means of interval analysis we find two disjoint compact subsets in a carefully chosen 3D cross section that can guarantee the existence of a topological horseshoe for the corresponding third-return Poincaré map. Numerical studies show that the Poincaré map expands in two directions. It justifiably indicates that there exists hyperchaos in the SHCG.

PACS numbers: 05.45.−a, 02.20.Pc

(Some figures in this article are in colour only in the electronic version)

1. Introduction

Over the past two decades, chaos has been found to be very useful to explain our uncertain world and it also has great potential in many engineering-oriented applied fields such as power systems protection, liquid mixing, information sciences. Especially, chaos application in encryption and communications has been intensively investigated since 1980s [1–6]. Recently, a field experiment on chaotic communications over a commercial fibre-optic channel shows that 'information can be transmitted at high bit rates using deterministic chaos in a manner that is robust to perturbations and channel disturbances unavoidable under real-world conditions' [6].

Hyperchaos introduced by Rössler [7] is usually characterized as a chaotic attractor with more than one positive Lyapunov exponent, that is, its dynamics expands not only as a line segment (one-dimensional expansion) but also as a small area (volume and so on) element (not less than two-dimensional expansion). Due to this, hyperchaos can exhibit much more complex dynamics than common chaos with only one positive Lyapunov exponent, so it is

[3] Author to whom correspondence should be addressed.

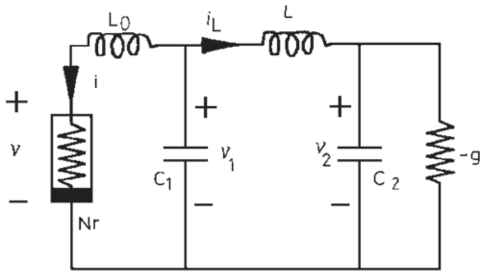

Figure 1. Saito hysteresis chaos generator.

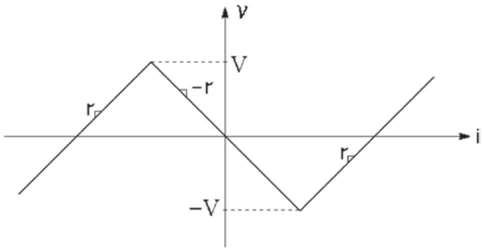

Figure 2. The characteristics of Nr.

believed that hyperchaos can play a better role in most applications of chaos. Therefore, hyperchaotic systems and their applications have recently become fields of active research [2, 4, 8–15].

However, before all these studies of hyperchaos, it must be ensured that the system is exactly hyperchaotic. Up to now, the only way to verify hyperchaos in continuous time systems in the literature is by calculating Lyapunov exponents. Unfortunately, this is not reliable sometimes because the unavoidable errors in computer simulations make numerical chaotic solutions deviate form their real orbits [16]. So we must find another method. Fortunately, the well-developed topological horseshoe theory provides a rigorous method to prove the existence of chaos, which has been investigated extensively in [17–21]. For hyperchaos, the Poincaré section is $\geqslant 3$ dimensions, which makes the problem too hard to find a horseshoe. However, for a 3D horseshoe, there is only a work on the chaotic Hodgkin–Huxley model [22], where the expansion is only in one direction.

In this paper, we propose a computer-assisted verification of hyperchaos in the well-known Saito hysteresis chaos generator (SHCG) by virtue of topological horseshoe theory. The model was proposed in [9], which is not only a fundamental work of a series of hyperchaotic systems [23–26], but also of importance to the research in hyperchaotic dynamics, encryption, private communications and so on [2, 4, 12–14].

This paper is organized as follows: in section 2 we revisit the hyperchaotic system; in section 3 we recall some aspects of horseshoe theory; in section 4 we present discussions about the existence of hyperchaos in the SHCG in terms of the horseshoe and in section 5 we draw conclusions.

2. The Saito hysteresis chaos generator

The SHCG is shown in figure 1, where the nonlinear resistor Nr is characterized by figure 2, i.e., a three-segment piecewise-linear v–i characteristic. Via the rescalings: $x = v_1/V$,

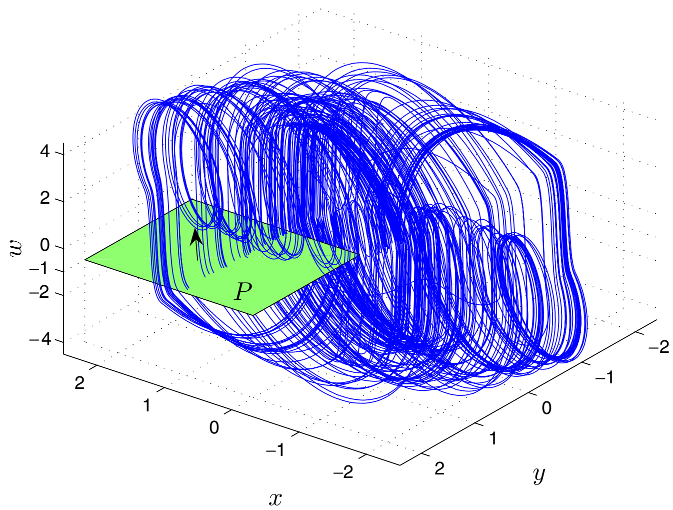

Figure 3. The phase plot of (1).

$y = v_2/V$, $z = ri_L/V$, $w = ri/V$, $t = t/(rC_1)$, $\epsilon = L_0/(r^2C_1)$, $\delta = rg/2$, $\rho = r^2C_1/L$ and $\gamma = C_1/C_2$, the dimensionless state equations of the SHCG are

$$\dot{x} = -z - w, \qquad \dot{y} = \gamma(2\delta y + z), \qquad \dot{z} = \rho(x - y), \qquad \epsilon\dot{w} = x - h(w) \tag{1}$$

where

$$h(w) = w - (|w + 1| - |w - 1|) \tag{2}$$

with x, y, z and w being the state variables and γ, δ, ρ and ϵ being the system parameters. Letting ϵ tend to zero, the nonlinear resistor Nr and the inductor L originate the jump phenomenon and hysteresis [9]. By varying the parameters of the SHCG, it is possible to generate a wide variety of dynamic behaviours such as periodic solutions, quasiperiodic solutions, chaos and hyperchaos.

In the studies of the SHCG, the parameters are often taken as $\gamma = 1$, $\delta = 1$, $\rho = 14$ and $\epsilon = 0.01$, and with these parameters the SHCG is hyperchaotic with its attractor illustrated in figure 3 [4, 9, 23]. To verify this, we will give detailed discussions of the horseshoe embedded in this hyperchaotic attractor in section 4. Before this, we review some aspects of a topological horseshoe.

3. Review of topological horseshoe theorem

Before studying the dynamics of the Poincaré map in the next section, we first recall some aspects of symbolic dynamics.

Let $S_m = \{0, 1, \ldots, m - 1\}$ be the set of nonnegative successive integer from 0 to $m - 1$. Let Σ_m be the collection of all bi-infinite sequences with their elements of Σ_m, i.e., every element s of Σ_m is of the following form:

$$s = \{\ldots, s_{-n}, \ldots, s_{-1}, s_0, s_1, \ldots, s_n, \ldots\}, \qquad s_i \in S_m.$$

Now consider another sequence

$$\bar{s} = \{\ldots, \bar{s}_{-n}, \ldots, \bar{s}_{-1}, \bar{s}_0, \bar{s}_1, \ldots, \bar{s}_n, \ldots\}, \qquad \bar{s}_i \in S_m.$$

The distance between s and $\bar{s}$ is defined as

$$d(s,\bar{s}) = \sum_{-\infty}^{+\infty} \frac{1}{2^{|i|}} \frac{|s_i - \bar{s}_i|}{1 + |s_i - \bar{s}_i|}. \tag{3}$$

With the distance defined as (3), Σ_m is a metric space, and it is well known that Σ_m is compact, totally disconnected and perfect [27]. A set having these properties is often defined as a Cantor set, such a Cantor set frequently appears in the characterization of complex structure of invariant set in a chaotic dynamical system.

Now define a m-shift map $\sigma : \Sigma_m \to \Sigma_m$ as follows:

$$\sigma(s)_i = s_{i+1}. \tag{4}$$

Proposition 1. *The shift map σ satisfies $\sigma(\Sigma_m) = \Sigma_m$ and is continuous. As a dynamical system defined on Σ_m, σ has the following properties:*

(i) σ has a countable infinity of periodic orbits consisting of orbits of all periods;
(ii) σ has an uncountable infinity of aperiodic orbits;
(iii) σ has a dense orbit.

For proofs of the above statements, see [27] (p 443). A consequence of proposition 1 is that the dynamics generated by the shift map σ is sensitive to initial conditions therefore is chaotic.

Now we will recall a result on horseshoes theory, which is essential for rigorous verification of chaoticity of the above hyperchaotic system (1) in terms of horseshoes.

Let X be a metric space, Q is a compact subset of X and $f : Q \to X$ is a map satisfying the assumption that there exist m mutually disjoint compact subsets $Q_1, Q_2, \ldots, Q_m$ of Q, the restriction of f to each Q_i, i.e., $f|Q_i$ is continuous.

Definition 1. *Let γ be a compact subset of Q, such that for each $1 \leqslant i \leqslant m$, $\gamma_i = \gamma \cap Q_i$ is nonempty and compact, then γ is called a connection with respect to $Q_1, Q_2, \ldots, Q_m$. Let F be a family of connections γs with respect to $Q_1, Q_2, \ldots, Q_m$ satisfying property $\gamma \in F \Rightarrow f(\gamma_i) \in F$. Then F is said to be an f-connected family with respect to $Q_1, Q_2, \ldots, Q_m$*

Theorem 1. *Suppose that there exists an f-connected family with F respect to $Q_1, Q_2, \ldots, Q_m$. Then there exists a compact invariant set $K \subset Q$, such that $f|K$ is semiconjugate to m-shift dynamics.*

Here, the semiconjugacy is conventionally defined as follows.

Definition 2. *Let M and N be topological spaces, and let $p: M \to M$ and $q: N \to N$ be continuous functions. We say that p is topologically semiconjugate to q, if there exists a continuous surjection $h: N \to M$ such that $ph = hq$.*

For details about the proof of the theorem, see [19], and for details of symbolic dynamics and horseshoe theory, see [27].

4. Cross section and Poincaré map

For the sake of finding the cross section and the Poincaré map, we need first to examine the equilibrium points and their properties, so that the cross section contains no equilibrium

Table 1. The equilibrium points of (1).

Equilibrium (o)	Eigenvalues (λ_1, $\alpha \pm \beta$i and λ_4)
$[0, 0, 0, 0]^T$	$[1.520\,88, 0.743\,938 + 5.229\,11\text{i}, 0.743\,938 - 5.229\,11\text{i}, 98.9912]^T$
$[-2, -2, 4, -4]^T$	$[0.546\,43, 0.222\,41 + 5.0826\text{i}, 0.222\,41 - 5.0826\text{i}, -98.991]^T$
$[2, 2, -4, 4]^T$	$[0.546\,43, 0.222\,41 + 5.0826\text{i}, 0.222\,41 - 5.0826\text{i}, -98.991]^T$

points and the Poincaré map makes sense. The equilibrium points and the eigenvalues of the linearization (Jacobian matrix) of (1) at these points are listed in table 1.

For clarity, we turn the coordinates of (1) a certain angle (0.301 414 366 1339 rad) via the transformation

$$\mathbf{x} = [x_1, x_2, x_3, x_4]^T = H[x, y, z, w]^T \tag{5}$$

where H is the following orthogonal matrix:

$$\begin{bmatrix} -0.009\,216\,137\,775\,232 & -0.296\,867\,818\,9175 & 0.954\,874\,107\,3543 & 0 \\ -0.004\,328\,087\,731\,346 & 0.954\,917\,559\,9503 & 0.296\,839\,554\,9032 & 0 \\ 0.999\,948\,163\,8871 & 0.001\,397\,064\,673\,894 & 0.010\,085\,521\,761\,38 & 0 \\ 0 & 0 & 0 & 1 \end{bmatrix} \tag{6}$$

so that the expanding directions of the following Poincaré map $\pi|a \cup b$ almost parallel the x_1ox_2 plane. It is obvious that $x_4 = w$.

Now consider the section hyperplane $P : x_4 = -1$, as shown in figure 3. The Poincaré map $\pi : P \to P$ is chosen as follows: For each $\mathbf{x} \in P$, $\pi(\mathbf{x})$ is taken to be the third-return point in P under the flow with the initial condition $\mathbf{x}$.

In this section hyperplane, we carefully take two boxes (hexahedrons): the first one is a with its eight vertices in term of (x_1, x_2, x_3) to be

$$\begin{aligned}
A_1 &= (-6.909\,544\,7256, -0.832\,251\,7553, 1.012\,482\,6036),\\
A_2 &= (-6.806\,751\,2482, -0.824\,982\,1705, 1.012\,482\,6036),\\
A_3 &= (-6.886\,743\,2633, -0.857\,305\,8601, 1.012\,482\,6036),\\
A_4 &= (-6.985\,051\,2072, -0.865\,743\,7710, 1.012\,482\,6036),\\
A_5 &= (-6.909\,544\,7256, -0.832\,251\,7553, 1.010\,482\,6036),\\
A_6 &= (-6.806\,751\,2482, -0.824\,982\,1705, 1.010\,482\,6036),\\
A_7 &= (-6.886\,743\,2633, -0.857\,305\,8601, 1.010\,482\,6036),\\
A_8 &= (-6.985\,051\,2072, -0.865\,743\,7710, 1.010\,482\,6036)
\end{aligned}$$

and the second one is b with its eight vertices in term of (x_1, x_2, x_3) to be

$$\begin{aligned}
B_1 &= (-6.116\,231\,2490, -0.860\,200\,3445, 1.012\,482\,6036),\\
B_2 &= (-5.781\,739\,3265, -0.841\,100\,3270, 1.012\,482\,6036),\\
B_3 &= (-5.969\,017\,5338, -0.864\,233\,8886, 1.012\,482\,6036),\\
B_4 &= (-6.186\,111\,1771, -0.877\,283\,5900, 1.012\,482\,6036),\\
B_5 &= (-6.116\,231\,2490, -0.860\,200\,3445, 1.010\,482\,6036),\\
B_6 &= (-5.781\,739\,3265, -0.8411003270, 1.010\,482\,6036),\\
B_7 &= (-5.969\,017\,5338, -0.864\,233\,8886, 1.010\,482\,6036),\\
B_8 &= (-6.186\,111\,1771, -0.877\,283\,5900, 1.010\,482\,6036),
\end{aligned}$$

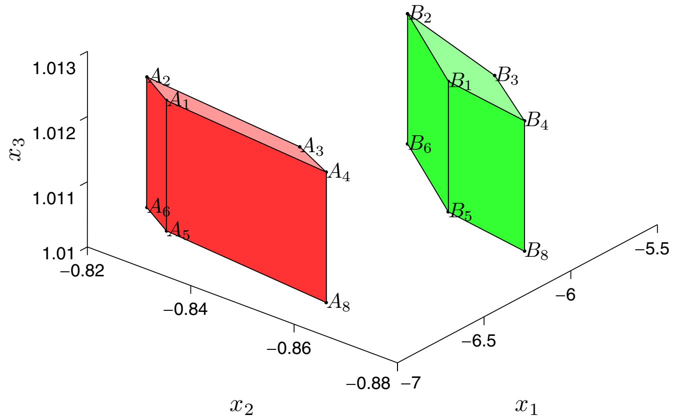

Figure 4. The position of box a and box b, where A_7 and B_7 are hidden behind.

as shown in figure 4. For box a, it is easy to see that the top surface $|A_1A_2A_3A_4|$ and the bottom surface $|A_5A_6A_7A_8|$ of a both parallel the x_1ox_2 plane, and they are both quadrangular. The other four surfaces of a called the side of a in the following discussions (indicated with S_a) are all rectangular. For box b, it has the same situation with a, and the side of b is indicated with S_b.

Under the Poincaré map π, a is sent to its image $a' = \pi(a)$ with

$$A'_1 = \pi(A_1), \qquad A'_2 = \pi(A_2), \qquad A'_3 = \pi(A_3), \qquad A'_4 = \pi(A_4),$$
$$A'_5 = \pi(A_5), \qquad A'_6 = \pi(A_6), \qquad A'_7 = \pi(A_7), \qquad A'_8 = \pi(A_8);$$

and b is sent to its image $b' = \pi(b)$ with

$$B'_1 = \pi(B_1), \qquad B'_2 = \pi(B_2), \qquad B'_3 = \pi(B_3), \qquad B'_4 = \pi(B_4),$$
$$B'_5 = \pi(B_5), \qquad B'_6 = \pi(B_6), \qquad B'_7 = \pi(B_7), \qquad B'_8 = \pi(B_8).$$

By means of interval analysis, the following statement can be obtained by numerical computations:

Proposition 2. *For the Poincaré map π corresponding to the cross sections $Q \triangleq a \cup b$, there exists a closed invariant set $\Lambda \subset Q$ for which $\pi|\Lambda$ is semiconjugate to the 2-shift map.*

Proof. To prove this statement, we will find two disjoint compact subsets of Q, such that the existence of a π-connected family can be easily derived.

The first subset takes a as shown in figures 5–7. From these figures, it is easy to see that the Poincaré map sends this subset to its image a' as follows:

- The top quadrangular $|A_1A_2A_3A_4|$ and the bottom quadrangular $|A_5A_6A_7A_8|$ are both expanded in two directions and wholly transversely intersect box a between $|A_1A_2A_3A_4|$ and $|A_5A_6A_7A_8|$ and box b between $|B_1B_2B_3B_4|$ and $|B_5B_6B_7B_8|$.
- The surface $|A'_1A'_2A'_3A'_4|$ is upon the surface $|A'_5A'_6A'_7A'_8|$.
- The side of a, i.e. S_a, is mapped outside of S_a and S_b, as shown in figure 6.

In this case, we say that the image $a' = \pi(a)$ lies wholly across the boxes a and b with respect to the sides of a and b, i.e. S_a and S_b.

The second subset takes b as shown in figures 8–10. Like the situation for subset, the Poincaré map sends this subset to its image b' as follows:

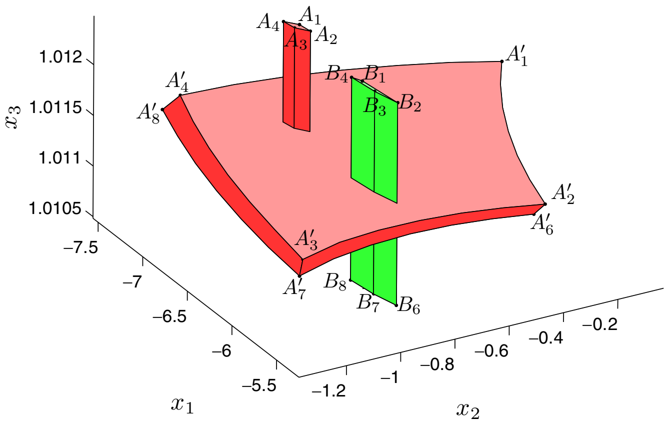

Figure 5. $a' = \pi(a)$ wholly across a and b.

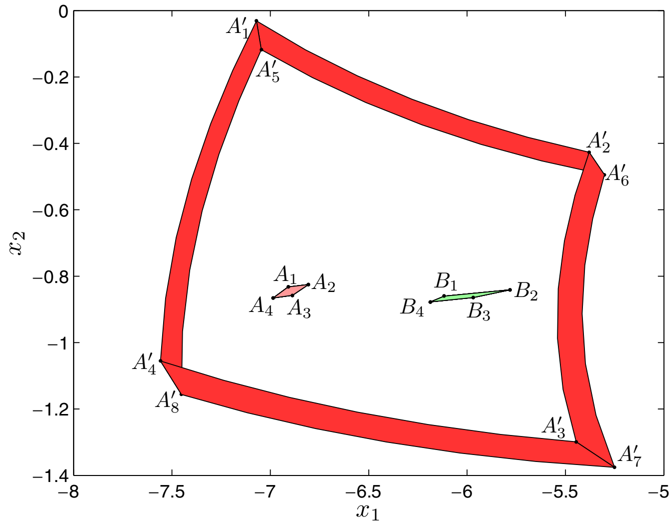

Figure 6. The top view of figure 5 with hiding $|A_1'A_2'A_3'A_4'|$ and $|A_5'A_6'A_7'A_8'|$.

- The top quadrangular $|B_1B_2B_3B_4|$ and the bottom quadrangular $|B_5B_6B_7B_8|$ are both expanded in two directions and wholly transversely intersect box a between $|A_1A_2A_3A_4|$ and $|A_5A_6A_7A_8|$ and box b between $|B_1B_2B_3B_4|$ and $|B_5B_6B_7B_8|$.
- The surface $|B_1'B_2'B_3'B_4'|$ is below the surface $|B_5'B_6'B_7'B_8'|$.
- The side of b, i.e. S_b, is mapped outside of S_a and S_b, as shown in figure 9.

In this case, we say that the image $a' = \pi(a)$ lies wholly across the boxes a and b with respect to the sides of a and b, i.e. S_a and S_b.

Note that the subsets a and b are mutually disjoint. It is easy to see from the whole acrossness of $\pi(a)$ and $\pi(b)$ with respect to both the sides of a and b that there exists a π-connected family with respect to a and b. In view of theorem 1, this means that the Poincaré map π is semiconjugate to a 2-shift map. □

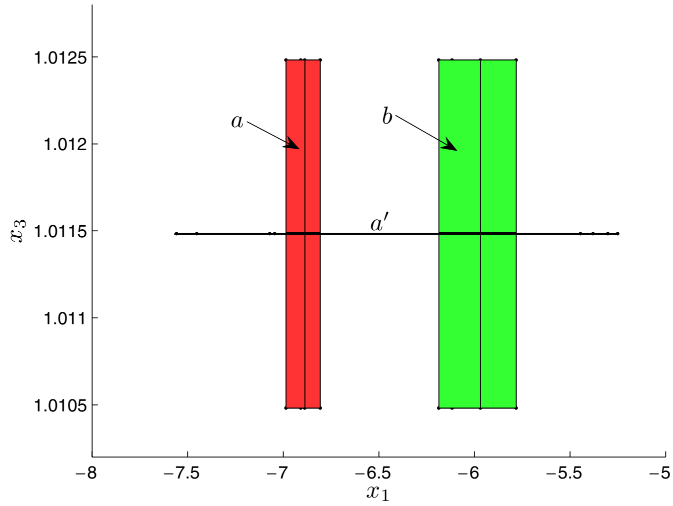

Figure 7. The side view of figure 5.

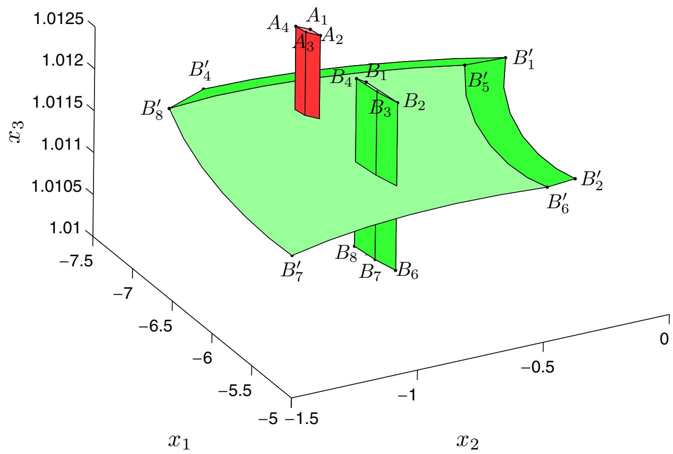

Figure 8. $b' = \pi(b)$ wholly across a and b.

Remark 1. In figures 5 and 8, the numerical computations show that the minimal distance between $\pi(S_a)$ and $S_a \cup S_b$ is greater than 0.23, the minimal distance between $\pi(S_b)$ and $S_a \cup S_b$ is also greater than 0.23, and the minimal distance from the top and bottom surfaces of a and b to their images is greater than 0.000 95. However, the maximal global error of computing the Poincaré map π is less than 1×10^{-9}, which is so small that figures 5–10 are believable. Our calculations are outlined as follows.

To calculate the Poincaré map with estimating the accuracy, we utilize the technique of interval arithmetic (for an overview, see [28]) by using an interval arithmetic package, called INTLAB: 'A MATLAB library for interval arithmetic routines', which is developed by Rump and available for WINDOWS and UNIX systems. For more details and downloading see http://www.ti3.tu-harburg.de/rump/intlab. In INTLAB, interval objects (e.g., interval numbers, interval vectors and interval matrices) work just like the common objects

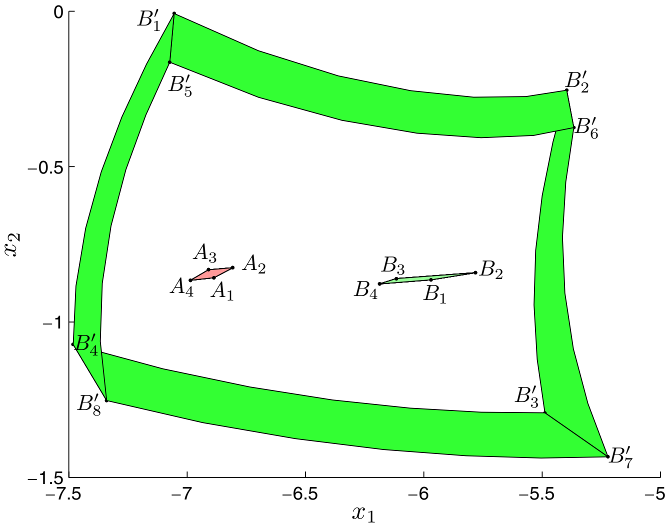

Figure 9. The top view of figure 8 with hiding $|B'_1B'_2B'_3B'_4|$ and $|B'_5B'_6B'_7B'_8|$.

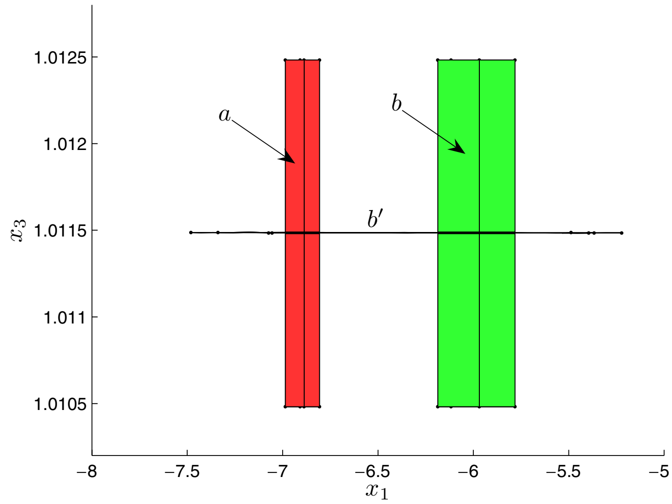

Figure 10. The side view of figure 8.

(e.g., numbers, vectors and matrices) of MATLAB. So, all variables in our programs are interval objects

Since (1) is a piecewise-linear system, it can be regarded as a switching system consisting of three simple continuous subsystems and two switching planes ($x_4 = +1$ and $x_4 = -1$). So, the Poincaré map π can be regarded as a composition of a series of sub-maps by the subsystems. Note that each subsystem is linear and has an equilibrium o with the eigenvalues of the system matrix being λ_1, $\alpha \pm \beta$i and λ_4 (table 1). The solutions can be described with

$$\mathbf{x}(t) = PDP^{-1}(\mathbf{x}(0) - o) + o, \tag{7}$$

where

$$D = \begin{pmatrix} e^{\lambda_1 t} & 0 & 0 & 0 \\ 0 & \cos(\alpha t) & \sin(\beta t) & 0 \\ 0 & -\sin(\beta t) & \cos(\alpha t) & 0 \\ 0 & 0 & 0 & e^{\lambda_4 t} \end{pmatrix}. \tag{8}$$

The main steps to compute the image of a point (a tiny interval vector) are as follows:

(i) Find eigenvalues and eigenvectors of the system matrix, calculate P^{-1} and estimate the error bounds [29].
(ii) For an initial interval vector $\mathbf{x}(0)$, solve the time t when it meets the switching planes and estimate the error bound.
(iii) Evaluate (7). Replace $\mathbf{x}(0)$ with $\mathbf{x}(t)$, go to the second step until all sub-maps are computed over.

To improve accuracy, we use long numbers with approximately 38 decimal digits. This slows down the performance of our code. It takes about 5 min to compute one tiny interval vector's map with 1.6 GHz Pentium M. Since a detailed interval analysis for the 3D Poincaré map will take an incredibly long time, we use a simplified interval analysis as follows. Figure 5 and 8 are computed by sampling two thousands of equally distributed tiny interval vectors from each surfaces of a and b. This takes four computers (Pentium IV, 3.0 GHz) about 200 h. The global errors are all less than 1×10^{-9}. We also calculate figures 5 and 8 by sampling about 10^6 points without error estimation. And the two results almost exactly match. These evidences strongly recommend that the global errors are acceptable.

Remark 2. The global picture of the images $\pi(a)$ and $\pi(b)$ suggests that $\pi|a$ and $\pi|b$ both expand in two directions. However, it is necessary to show local expansions of $\pi|\Lambda$. To confirm this, we compute short-term Lyapunov exponents (SLEs) of 2×10^5 orbits from randomly chosen points in the intersection set of boxes a and b and their images to $\pi(Q)$ with QR-based method [30]. The first two initial vectors for the first two SLEs parallel the section hyperplane. After days of computation, the minima of the first two Lyapunov exponents are approximately 0.340 and 0.075, and the last one is near -95. This suggests that the local expansions are in two directions. Thereby, it justifiably indicates an evidence that the attractor illustrated in figure 3 is hyperchaotic.

Remark 3. Since the image of the Poincaré map continuously depends on the parameters γ, δ, ρ and ϵ, it can be seen that for them sufficiently close to 1, 1, 14 and 0.01, respectively, the corresponding Poincaré map still has a π-connected family with respect to some two sets such as a and b discussed above, thus having a horseshoe and consequently exhibiting hyperchaos.

Remark 4. As was mentioned in the introduction, the numerical accuracy of a Lyapunov exponent may not be high enough to decide whether or not it is positive. However, the Lyapunov exponents of the periodic orbits embedded in a given attractor can be computed with extremely high accuracy. Therefore, one can also draw partial conclusions on Lyapunov exponents from the embedded periodic orbits, and some approaches have been proposed to find unstable periodic orbits in a chaotic attractor [31].

5. Conclusions

In this paper, we propose a computer-assisted verification of hyperchaos in the well-known Saito hysteresis chaos generator (SHCG) by virtue of topological horseshoe theory. To the best knowledge of the authors, it seems the first report about finding a horseshoe in a hyperchaotic system, which tells us that it may be possible in practice to prove the existence of hyperchaos by the topological horseshoe theory as we do for chaos with only one positive Lyapunov exponent.

Acknowledgments

The authors are indebted to the anonymous referees for their valuable comments. This work was partially supported by the Foundation for Young Teachers (A2005-15) and the Automation Project of Chongqing University of Posts and Telecommunications. The second author is supported in part by the Program for New Century Excellent Talents in University.

References

[1] Ushio T 1996 Control of chaotic synchronization in composite systems with applications to secure communication systems *IEEE Trans. Circuits Syst.* I **43** 500–3
[2] Zhang Y *et al* 1999 Hyperchaotic synchronization scheme for digital speech communication *Electron. Lett.* **35** 2087–9
[3] Dai M, Zhang Y, Hua Y, Ni W and Du G 1998 Implementation of secure digital communication by hyperchaotic synchronization *Electron. Lett.* **34** 951–3
[4] Kunz M and Vogelsang K 1999 Synchronizing hyperchaotic systems by observer design *IEEE Trans. Circuits Systems* II **46** 478
[5] Lian K-Y, Chiang T-S, Chiu C-S and Liu P 2001 Synthesis of fuzzy model-based designs to synchronization and secure communications for chaotic systems *IEEE Trans. Systems Man Cybern.* B **31** 66–83
[6] Argyris A, Syvridis D, Larger L, Annovazzi-Lodi V, Colet P, Fischer I, Garcia-Ojalvo J, Mirasso C R, Pesquera L and Alan Shore K 2005 Chaos-based communications at high bit rates using commercial fibre-optic links *Nature* **438** 343–6
[7] Rössler O E 1979 An equation for hyperchaos *Phys. Lett.* A **71** 155–7
[8] Nikolov S and Clodong S 2004 Occurrence of regular, chaotic and hyperchaotic behavior in a family of modified rossler hyperchaotic systems *Chaos Solitons Fractals* **22** 407–31
[9] Saito T 1990 An approach toward higher dimensional hysteresis chaos generators *IEEE Trans. Circuits Syst.* I **37** 399–409
[10] Matsumoto T, Chua L O and Kobayashi K 1986 Hyperchaos: laboratory experiment and numerical confirmation *IEEE Trans. Circuits Syst.* **33** 1143–7
[11] Yanchuka S and Kapitaniak T 2001 Chaos–hyperchaos transition in coupled Rössler systems *Phys. Lett.* A **290** 139–44
[12] Storace M and Bizzarri F 2001 Basic bifurcation analysis of a hysteresis oscillator *Int. J. Circuit Theory Appl.* **29** 343–366
[13] Miller D A and Grassi G 2001 Experimental realization of observer-based hyperchaos synchronization *IEEE Trans. Circuits Syst.* I **48** 366
[14] Grassi G and Mascolo S 1999 A system theory approach for designing cryptosystems based on hyperchaos *IEEE Trans. Circuits Syst.* I **46** 1135
[15] Takahashi Y, Nakano H and Saito T 2004 A simple hyperchaos generator based on impulsive switching *IEEE Trans. Circuits Syst.* II **51** 468–72
[16] Sauer T, Grebogi C and Yorke J A 1997 How long do numerical chaotic solutions remain valid? *Phys. Rev. Lett.* **79** 59–62
[17] Szymczak A 1996 The Conley index and symbolic dynamics *Topology* **35** 287–99
[18] Zgliczyński P and Gidea M 2004 Covering relations for multidimensional dynamical systems *J. Diff. Eqns* **202** 32–58
[19] Yang X-S and Tang Y 2004 Horseshoes in piecewise continuous maps *Chaos Solitons Fractals* **19** 841–5
[20] Yang X-S 2004 Metric horseshoes *Chaos Solitons Fractals* **20** 1149–56
[21] Yang X-S, Li H and Huang Y 2005 A planar topological horseshoe theory with applications to computer verifications of chaos *J. Phys. A: Math. Gen.* **38** 4175–85
[22] Guckenheimer J and Oliva R A 2002 Chaos in the Hodgkin–Huxley model *SIAM J. Appl. Dyn. Syst.* **1** 105–14

[23] Arena P, Baglio S, Fortuna L and Manganaro G 1995 Hyperchaos from cellular neural networks *Electron. Lett.* **31** 250–1

[24] Tsubone T and Saito T 1998 Hyperchaos from a 4-d manifold piecewise-linear system *IEEE Trans. Circuits Syst.* I **45** 889–94

[25] Li Q, Yang X-S and Yang F 2005 Hyperchaos in Hopfield-type neural networks *Neurocomputing* **67** 275–80

[26] Yang X-S and Li Q 2006 Horseshoe chaos in cellular neural networks *Int. J. Bifurcation Chaos*

[27] Wiggins S 1990 *Introduction to Applied Nonlinear Dynamical Systems and Chaos* (New York: Springer)

[28] Alefeld G and Mayer G 2000 Interval analysis: theory and applications *J. Comput. Appl. Math.* **121** 421–64

[29] Rump Siegfried M 2001 Computational error bounds for multiple or nearly multiple eigenvalues *Linear Algebr. Appl.* **324** 209–26

[30] Eckmann J P and Ruelle D 1985 Ergodic theory of chaos and strange attractors *Rev. Mod. Phys.* **57** 617–56

[31] Eckmann J P and Ruelle D 2001 Detecting unstable periodic orbits in chaotic continuous-time dynamical systems *Phys. Rev.* E **64** 026214